

Dynamic Contrast-enhanced MRI Quantification of Altered Vascular Permeability in Autoimmune Encephalitis

So-Hyun Ji, MD* • Roh-Eul Yoo, MD, PhD* • Seung Hong Choi, MD, PhD • Woo Jin Lee, MD, PhD • Soon Tae Lee, MD, PhD • Young Hun Jeon, MD • Kyu Sung Choi, MD, PhD • Ji Ye Lee, MD • Inpyeong Hwang, MD • Kyoung Mi Kang, MD, PhD • Tae Jin Yun, MD, PhD



From the Department of Radiology, National Cancer Center, Goyang, Republic of Korea (S.H.J.); Departments of Radiology (R.E.Y., S.H.C., J.Y.L., I.H., K.M.K., T.J.Y.) and Neurology (S.T.L.), Seoul National University College of Medicine, Seoul, Republic of Korea; Department of Radiology, Seoul National University Hospital, Seoul National University College of Medicine, 101 Daehangno, Jongno-gu, Seoul 03080, Republic of Korea (R.E.Y., S.H.C., Y.H.J., K.S.C., J.Y.L., I.H., K.M.K., T.J.Y.); Center for Nanoparticle Research, Institute for Basic Science, and School of Chemical and Biological Engineering, Seoul National University, Seoul, Republic of Korea (S.H.C.); and Department of Neurology, Seoul National University Bundang Hospital, Seongnam, Republic of Korea (W.J.L.). Received March 20, 2023; revision requested May 19; final revision received January 3, 2024; accepted February 7. Address correspondence to S.H.C. (email: verocay1@snu.ac.kr).

Supported by Basic Science Research Program through the National Research Foundation of Korea, funded by the Ministry of Science, ICT and Future Planning (NRF-2020R1A2C2008949, RS-2023-00242754, RS-2023-00224382, and RS-2023-00207783); the National Research Foundation of Korea grant, funded by the Ministry of Science and ICT (NRF-2021R1A4A1028713 and NRF-2023R1A2C3003250); Samsung Research Funding and Incubation Center of Samsung Electronics (project no. SRFC-IT2201-04); the Seoul National University Hospital GE Center (grant no. 1820230040); the Institute for Basic Science (IBS-R006-D1); and the Seoul National University Hospital Research Fund (grant no. 0320230270).

*S.H.J. and R.E.Y. contributed equally to this work.

Conflicts of interest are listed at the end of this article.

See also the editorial by Filippi and Rocca in this issue.

Radiology 2024; 310(3):e230701 • <https://doi.org/10.1148/radiol.230701> • Content codes:  

Background: Blood-brain barrier (BBB) permeability change is a possible pathologic mechanism of autoimmune encephalitis.

Purpose: To evaluate the change in BBB permeability in patients with autoimmune encephalitis as compared with healthy controls by using dynamic contrast-enhanced (DCE) MRI and to explore its predictive value for treatment response in patients.

Materials and Methods: This single-center retrospective study included consecutive patients with probable or possible autoimmune encephalitis and healthy controls who underwent DCE MRI between April 2020 and May 2021. Automatic volumetric segmentation was performed on three-dimensional T1-weighted images, and volume transfer constant (K^{trans}) values were calculated at encephalitis-associated brain regions. K^{trans} values were compared between the patients and controls, with adjustment for age and sex with use of a nonparametric approach. The Wilcoxon rank sum test was performed to compare K^{trans} values of the good (improvement in modified Rankin Scale [mRS] score of at least two points or achievement of an mRS score of ≤ 2) and poor (improvement in mRS score of less than two points and achievement of an mRS score > 2) treatment response groups among the patients.

Results: Thirty-eight patients with autoimmune encephalitis (median age, 38 years [IQR, 29–59 years]; 20 [53%] female) and 17 controls (median age, 71 years [IQR, 63–77 years]; 12 [71%] female) were included. All brain regions showed higher K^{trans} values in patients as compared with controls ($P < .001$). The median difference in K^{trans} between the patients and controls was largest in the right parahippocampal gyrus ($25.1 \times 10^{-4} \text{ min}^{-1}$ [95% CI: 17.6, 43.4]). Among patients, the poor treatment response group had higher baseline K^{trans} values in both cerebellar cortices ($P = .03$), the left cerebellar cortex ($P = .02$), right cerebellar cortex ($P = .045$), left cerebral cortex ($P = .045$), and left postcentral gyrus ($P = .03$) than the good treatment response group.

Conclusion: DCE MRI demonstrated that BBB permeability was increased in all brain regions in patients with autoimmune encephalitis as compared with controls, and baseline K^{trans} values were higher in patients with poor treatment response in the cerebellar cortex, left cerebral cortex, and left postcentral gyrus as compared with the good response group.

© RSNA, 2024

Supplemental material is available for this article.

Autoimmune encephalitis is a neuroinflammatory disease with subacute memory loss, psychiatric symptoms, and seizures, frequently associated with coexisting tumors (1). Advances in research in the past 10 years have identified various biomarkers and clinical syndromes, long after it was first described as “paraneoplastic limbic encephalitis” by Corsellis et al in 1968 (2). Although the exact prevalence of autoimmune encephalitis remains elusive, the reported incidence has increased over time with growing awareness of the associated antibodies and biomarkers. Specifically, the prevalence of autoimmune encephalitis per 100 000 population as of 2014 was reported to be 13.7, which

was not substantially different from that of all infectious encephalitis (11.6) or the viral subcategory (8.3) (3). However, the diagnosis is clinically challenging due to its diverse clinical features that can mimic other pathologic abnormalities. Furthermore, imaging findings of autoimmune encephalitis are nonspecific and inconsistent with disease severity. Specifically, structural MRI frequently fails to depict any abnormalities in patients with anti-*N*-methyl-D-aspartate (NMDA) receptor encephalitis, with the reported incidence of positive findings being only 50%, even in comatose patients (4–7).

In autoimmune encephalitis, autoantibodies in patients’ sera and cerebrospinal fluid targeting brain tissues

Abbreviations

BBB = blood-brain barrier, DCE = dynamic contrast enhanced, FLAIR = fluid-attenuated inversion recovery, K^{trans} = volume transfer constant, mRS = modified Rankin Scale, NMDA = *N*-methyl-D-aspartate

Summary

Dynamic contrast-enhanced MRI demonstrated that volume transfer constant (K^{trans}) values in all brain regions were higher in patients with autoimmune encephalitis, and a higher baseline K^{trans} was associated with poor treatment response.

Key Results

- In a retrospective study of 38 patients with autoimmune encephalitis and 17 healthy controls undergoing dynamic contrast-enhanced MRI, volume transfer constant (K^{trans}) values in all brain regions were higher in patients as compared with controls, with the largest median difference in the right parahippocampal gyrus ($25.1 \times 10^{-4} \text{ min}^{-1}$ [95% CI: 17.6, 43.4]; $P < .001$).
- Among patients, poor treatment responders had higher baseline K^{trans} values than good responders in both cerebellar cortices ($P = .03$), the left cerebellar cortex ($P = .02$), right cerebellar cortex ($P = .045$), left cerebral cortex ($P = .045$), and left postcentral gyrus ($P = .03$).

cause neuronal circuit dysfunction or damage brain tissues (8–10). Accumulating evidence from recent animal and human studies has suggested that the entry of immune cells into cerebrospinal fluid via meningeal lymphatic vessels and blood-brain barrier (BBB) disruption plays a key role in the pathogenesis of autoimmune encephalitis (11–16). When cytokines or chemokines trigger BBB disruption, autoantibodies and immune cells in cerebrospinal fluid and blood can cross the leaky BBB and enter the brain parenchyma (11–14,16).

Dynamic contrast-enhanced (DCE) MRI is a useful method for quantitative assessment of the functional integrity of the BBB (17,18). Using DCE MRI, previous studies have shown BBB functional abnormalities in many central nervous system pathologies, ranging from large leakage in central nervous system tumors and multiple sclerosis to subtle leakage in small vessel disease, traumatic brain injury, migraine, and Alzheimer disease (19–23).

To our knowledge, no human study has explored the potential of DCE MRI to reflect subtle BBB disruption in autoimmune encephalitis with use of quantitative parameters of DCE MRI. Thus, the purpose of this study was to evaluate the change in BBB permeability in patients with autoimmune encephalitis as compared with healthy controls by using DCE MRI and to explore its predictive value for treatment response in patients.

Materials and Methods

This retrospective study was approved by the institutional review board of Seoul National University Hospital (no. H-2208-198-1358), and the requirement for informed consent was waived due to its retrospective nature.

Study Sample

Consecutive patients with suspected autoimmune encephalitis who underwent a dedicated MRI protocol for the

evaluation of BBB permeability (including DCE MRI) between April 2020 and May 2021 were selected from a radiology report database of a tertiary referral hospital, Seoul National University Hospital. Patients were excluded due to different or uncertain diagnosis, detection of both NMDA receptor and myelin oligodendrocyte glycoprotein autoantibodies, baseline MRI performed after initial treatment, subtypes of small number for statistical analysis, and failed image postprocessing. All of the images in patients excluded due to failed automatic segmentation were reviewed by a neuroradiologist (S.H.J., with 5 years of experience in neuroradiology) blinded to clinical information for the possible causes of the automatic segmentation failure.

All healthy volunteer controls were reported in a previous study (22), which evaluated altered vascular permeability in migraine-associated brain regions with use of DCE MRI.

MRI Scan Acquisition

All baseline (pretreatment) and follow-up MRI studies were performed with a 3.0-T imaging unit using a 32-channel head coil (Discovery 750; GE HealthCare). The optimal protocol included pre- and postcontrast three-dimensional fast spoiled gradient-echo and postcontrast three-dimensional black-blood T1-weighted fat-suppressed Cube motion sensitization–driven equilibrium sequences with multiplanar reconstructions of sagittal, coronal, and transverse T1-weighted images, T2 fluid-attenuated inversion-recovery (FLAIR) images, and DCE MRI scans (Table S1). DCE MRI was performed after intravenous injection of gadobutrol (Gadovist; Bayer Schering Pharma) (0.1 mmol/L/kg) with a power injector (Spectris; Medrad) at a rate of 4 mL/sec.

MRI Postprocessing and Data Analysis

All image analyses were performed by one neuroradiologist (S.H.J.) blinded to clinical information under the supervision of an expert neuroradiologist (R.E.Y., with 12 years of experience in neuroradiology). Details on the generation of 20 analytic masks and volume transfer constant (K^{trans}) maps are provided in Appendix S1 and Table S2. The K^{trans} map and brain region masks were coregistered using NordiCE (version 2.3.12; NordicNeuroLab) (Fig 1). For each analytic mask, K^{trans} values were calculated on a pixel-by-pixel basis on every axial image. Finally, the values were pooled to obtain mean values of the analytic mask areas. In addition, for patients with positive findings at structural MRI, regions of interest were manually selected on T2 FLAIR and postcontrast black-blood T1-weighted images for the comparison of K^{trans} values among three different regions: (a) T2 FLAIR hyperintense lesions with contrast enhancement (mean area, $13 \text{ cm}^2 \pm 18$ [SD]), (b) T2 FLAIR hyperintense lesions without contrast enhancement ($122 \text{ cm}^2 \pm 137$), and (c) normal-appearing regions ($52 \text{ cm}^2 \pm 47$). Normal-appearing regions were selected as the most approximate mirror image regions of normal appearance.

Treatment Response Analysis

Of the final study sample, the treatment responses of all patients with autoimmune encephalitis with treatment and

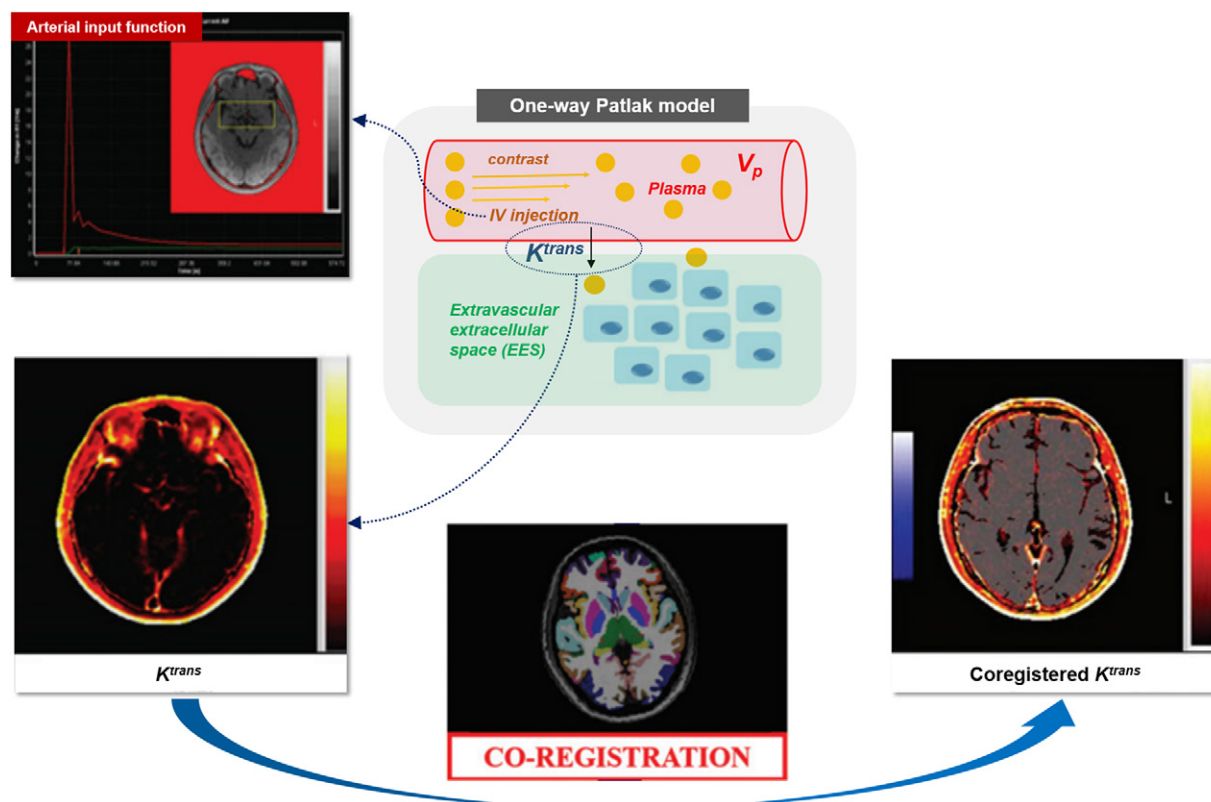


Figure 1: Schematic illustration of study design using dynamic contrast-enhanced MRI and coregistration of volume transfer constant (K^{trans}) maps with region masks. Intravenously injected low-molecular-weight contrast agent (yellow circles) within the blood vessel extravasates into the extravascular extracellular space through the impaired blood-brain barrier. The K^{trans} represents the rate at which the contrast agent is delivered to the extravascular extracellular space per volume of tissue. The arterial input function graph is automatically extracted at the level of the middle cerebral artery (yellow box within the arterial input function graph) using an automatic searching algorithm. Subsequently, the K^{trans} maps are derived using the one-way two-compartment Patlak model. Finally, the K^{trans} maps are coregistered with automatically segmented autoimmune encephalitis-associated brain regions. IV = intravenous, V_p = fractional plasma volume.

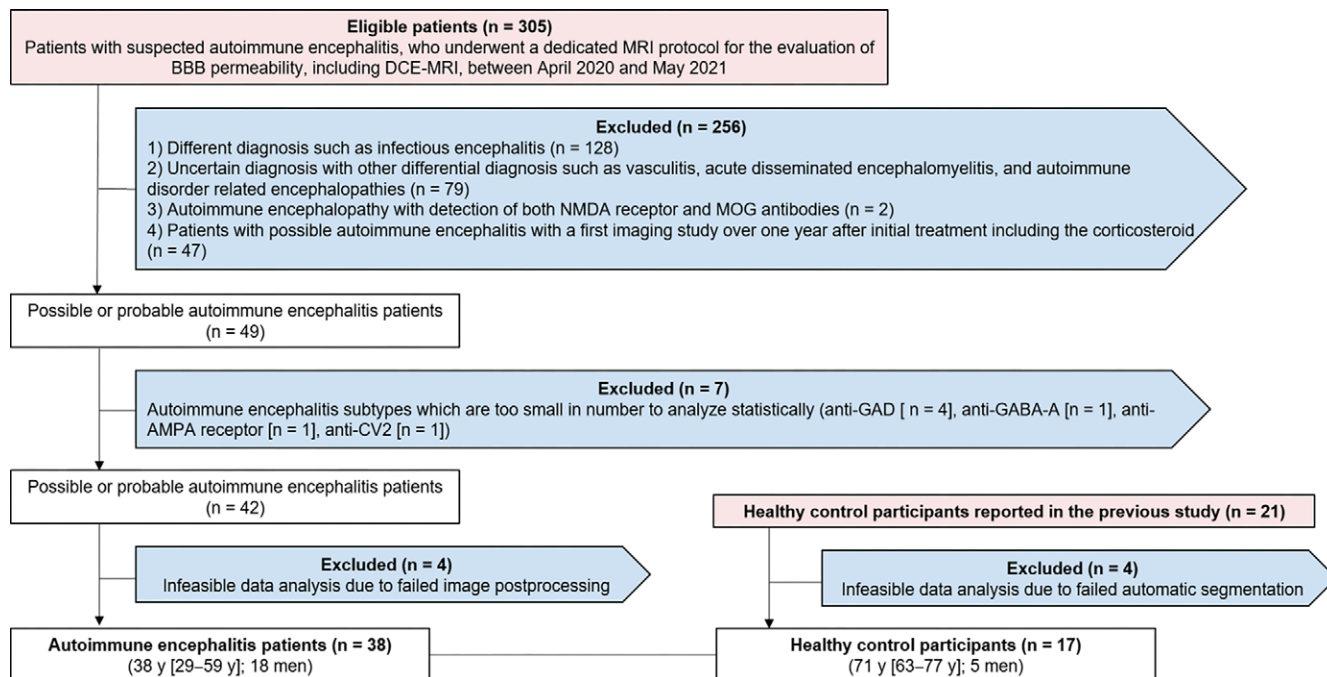


Figure 2: Flowchart shows patient inclusion in the study. AMPA = alpha-amino-3-hydroxy-5-methyl-4-isoxazolepropionic acid, BBB = blood-brain barrier, DCE = dynamic contrast enhanced, GABA-A = gamma-aminobutyric acid type A, GAD = glutamic acid decarboxylase, MOG = myelin oligodendrocyte glycoprotein, NMDA = N-methyl-D-aspartate.

Table 1: Baseline Clinical Characteristics

Variable	Patients (n = 38)	Controls (n = 17)	P Value
Age (y)*	38 (29–59)	71 (63–77)	<.001
Sex			.25
F	20 (53)	12 (71)	
M	18 (47)	5 (29)	
Time between clinical onset and baseline MRI scan acquisition (mo)*	3.0 (1.0–9.8)	NA	NA
Follow-up imaging	15 (39)	NA	NA
Time between baseline and follow-up imaging (mo)*	3.5 (2.3–5.0)	NA	NA
Baseline mRS score*	3.0 (1.3–4.0)	NA	NA
Treatment response†			
Good	29	NA	NA
Poor	6	NA	NA

Note.—Unless otherwise indicated, data are numbers of patients, with percentages in parentheses. NA = not available.

* Data are medians, with IQRs in parentheses.

† Based on the modified Rankin Scale (mRS) and the Clinical Assessment Scale in Autoimmune Encephalitis. Specifically, good treatment response was defined at the last follow-up period as improvement in mRS score of at least two points or achievement of an mRS score of 2 or less (24). Poor treatment response was defined as improvement in mRS score of less than two points and achievement of an mRS score higher than 2.

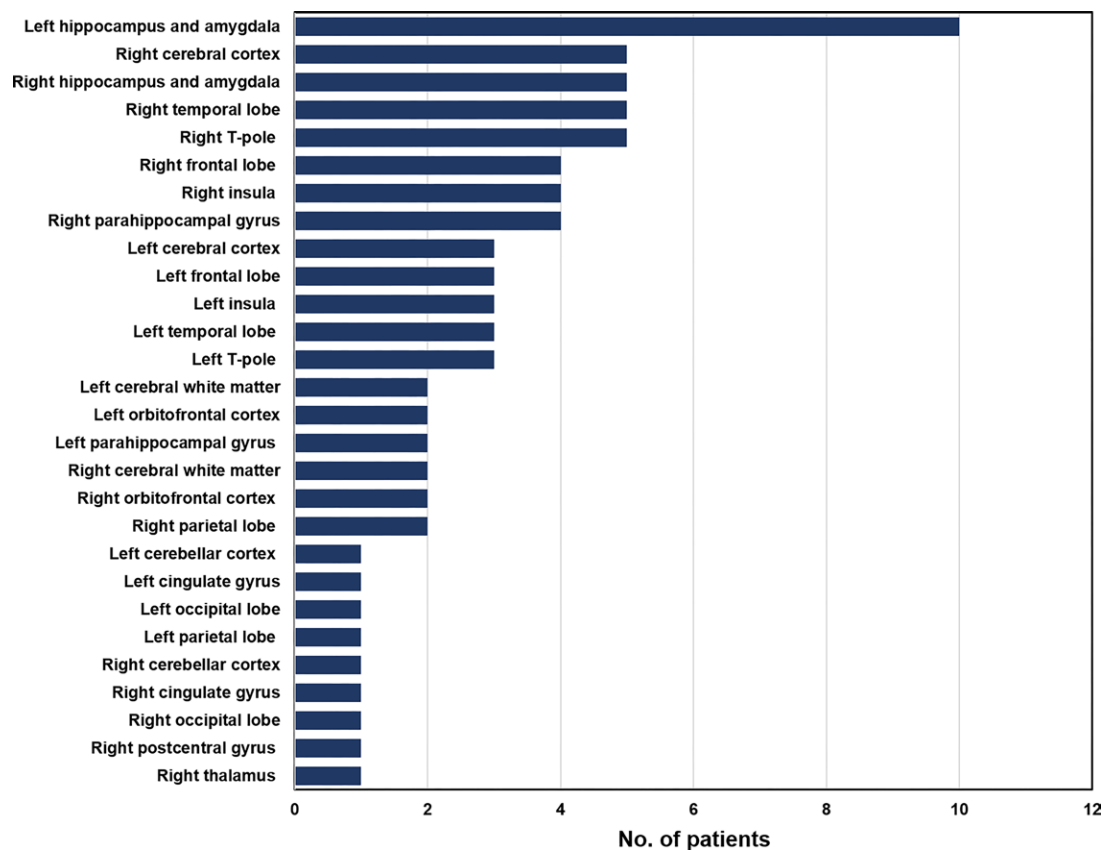


Figure 3: Bar graph shows number of patients with positive findings at structural MRI with high signal intensity on T2 fluid-attenuated inversion recovery images in the total patient group. T-pole represents a region including the superior, middle, and inferior temporal gyrus and the temporal pole.

accessible electronic medical records were evaluated by an expert neurologist (W.J.L., with 11 years of experience in neurology) based on the modified Rankin Scale (mRS) and the Clinical Assessment Scale in Autoimmune Encephalitis. Specifically, good treatment response was defined at the last

follow-up period as improvement in mRS score of at least two points or achievement of an mRS score of 2 or less (24). Poor treatment response was defined as improvement in mRS score of less than two points and achievement of an mRS score higher than 2.

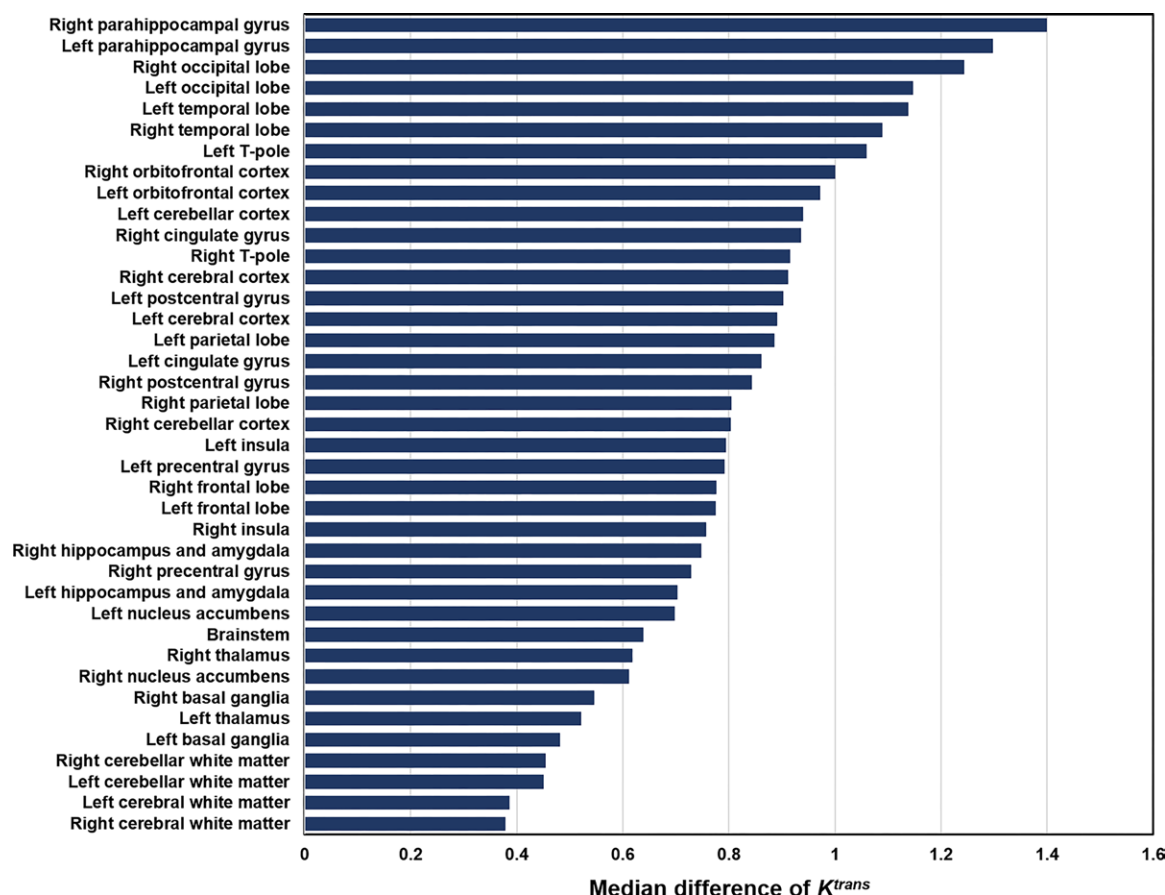


Figure 4: Bar graph shows median difference in volume transfer constant (K^{trans}) values in all brain regions in the total patient group (in descending order) as compared with controls. The median difference in K^{trans} is expressed as $\log(K^{trans} \times 10^4)$. T-pole represents a region including the superior, middle, and inferior temporal gyrus and the temporal pole.

Statistical Analysis

RStudio (version 2021.09.2 + 382 Ghost Orchid; Posit Software) and SAS (version 9.4; SAS Institute) were used for statistical analysis. A post hoc power calculation indicated that a sample size of 55 (38 patients and 17 healthy controls) had 90% power to detect an effect size of 0.99 in regional K^{trans} using a two-sided Mann-Whitney U test with a significance level of .05 based on the effect size, which was calculated by using the mean and SD estimated from the sample size and the median with IQR of K^{trans} values in a previous study (25,26). The normality of the data was assessed using the Shapiro-Wilk test. Because not all the data followed a normal distribution, nonparametric tests were used, and the data are reported as medians with IQRs. The Hodges-Lehmann estimator was used to estimate the median differences along with their 95% CIs.

Clinical data were compared between the patient and control groups with use of the Fisher exact test for categorical variables and the Wilcoxon rank-sum test for continuous variables. The Kruskal-Wallis test, followed by post hoc tests with Bonferroni correction for multiple comparisons ($n = 3$), was used for comparisons of K^{trans} values among three regions on structural MRI in the patient group. K^{trans} values were compared between the patient and control groups, with adjustment for the differences in age and sex using a nonparametric approach

for covariate adjustment (27). The Wilcoxon signed-rank test was used to evaluate the changes in K^{trans} from baseline in the patient group. The Wilcoxon rank sum test was performed to compare K^{trans} values of the good and poor treatment response groups within the patient group. P values were adjusted for multiple comparisons for both patients versus healthy controls as well as for good versus poor responders and baseline versus follow-up imaging within the patient group, with the use of Bonferroni correction ($n = 58$). The Wilcoxon rank sum test and Fisher exact test were used to compare demographic and clinical factors reported to be associated with poor treatment response in the previous literature: (a) Anti-NMDA Receptor Encephalitis One-Year Functional Status score, (b) age older than 60 years, (c) infratentorial lesion at structural MRI, and (d) antibody subtype (28,29). The Spearman rank correlation analysis and Wilcoxon rank sum test were used to correlate baseline K^{trans} values and various clinical factors, including disease duration (the time between clinical onset and baseline DCE MRI), baseline mRS scores, cerebrospinal fluid pleocytosis, albumin ratio, and the presence of electroencephalographic abnormalities. The Kruskal-Wallis test, followed by post hoc tests with Bonferroni correction for multiple comparisons, and the Fisher exact test were used to compare K^{trans} values and clinical data among three different subtypes of autoimmune encephalitis. Intraclass correlation

coefficients of the whole-brain K^{trans} quantification were calculated to determine the test-retest reproducibility. $P < .05$ was considered indicative of a statistically significant difference.

Results

Baseline Characteristics of the Study Sample

Of 305 consecutive patients with suspected autoimmune encephalitis (425 studies), 263 were excluded due to different diagnosis ($n = 128$), uncertain diagnosis with other differential diagnosis ($n = 79$), patients with possible autoimmune encephalitis with a first imaging study more than 1 year after initial treatment ($n = 47$), subtypes of small number for statistical analysis ($n = 7$), and autoimmune encephalopathy with detection of both NMDA receptor and myelin oligodendrocyte glycoprotein antibodies ($n = 2$) (Fig 2). Of the remaining 42 patients, four were excluded due to the failure of image postprocessing (two with the failure of automatic brain segmentation because of motion artifacts and two with the failure of image coregistration using NordiICE). Among the 21 healthy controls, four were excluded due to failed automatic brain segmentation. After exclusions, this study included 38 patients with autoimmune encephalitis (median age, 38 years [IQR, 29–59 years]; 20 [53%] female, 18 [47%] male) and 17 healthy controls (median age, 71 years [IQR, 63–77 years]; 12 [71%] female, five [29%] male) (Table 1). The median age of patients was younger than that of healthy controls ($P < .001$). Follow-up DCE MRI was performed in 15 of the 38 patients (39%), with a median interval of 3.5 months (IQR, 2.3–5.0 months).

The patient group consisted of patients with anti-leucine-rich glioma-inactivated 1 ($n = 7$), anti-NMDA receptor ($n = 10$), and antibody-negative but probable autoimmune encephalitis ($n = 21$) (Table S3). The median age of patients with

Table 2: Comparison of Regional K^{trans} Between Patient and Healthy Control Groups

Brain Region and Laterality	Patients ($\times 10^{-4} \text{ min}^{-1}$)	Controls ($\times 10^{-4} \text{ min}^{-1}$)
Left nucleus accumbens	6.41 (3.62–15.9)	1.15 (0.897–2.24)
Right nucleus accumbens	5.03 (4.31–14.1)	0.975 (0.794–1.93)
Left basal ganglia	3.98 (3.10–10.8)	0.953 (0.666–1.53)
Right basal ganglia	4.62 (3.70–8.99)	1.04 (0.732–1.85)
Left cerebellar cortex	11.2 (7.14–24.3)	1.48 (1.17–2.67)
Right cerebellar cortex	8.14 (6.07–14.3)	1.22 (0.864–2.39)
Left cerebellar white matter	3.88 (2.52–7.73)	0.696 (0.504–1.25)
Right cerebellar white matter	3.65 (2.49–8.00)	0.645 (0.496–1.18)
Left cerebral cortex	9.34 (8.17–22.3)	1.82 (1.15–2.38)
Right cerebral cortex	10.0 (7.77–21.0)	1.83 (1.25–2.97)
Left cerebral white matter	3.20 (2.56–7.19)	0.765 (0.477–0.988)
Right cerebral white matter	3.20 (2.34–6.00)	0.805 (0.518–1.14)
Left cingulate gyrus	9.66 (6.72–39.5)	1.77 (0.962–2.93)
Right cingulate gyrus	10.2 (9.03–30.5)	1.68 (1.08–3.90)
Left frontal lobe	7.19 (5.98–18.4)	1.32 (0.968–1.93)
Right frontal lobe	7.39 (5.63–13.3)	1.31 (0.968–2.43)
Left hippocampus and amygdala	6.74 (4.77–29.5)	1.22 (0.985–2.61)
Right hippocampus and amygdala	7.15 (4.53–17.1)	1.31 (0.763–3.02)
Left insula	7.89 (5.86–36.8)	1.42 (0.907–2.25)
Right insula	7.30 (4.83–50.6)	1.41 (0.861–2.16)
Left occipital lobe	17.3 (14.7–34.9)	3.15 (1.90–4.54)
Right occipital lobe	21.5 (16.7–41.7)	3.27 (1.91–4.58)
Left orbitofrontal cortex	11.9 (8.17–31.7)	2.26 (1.62–2.96)
Right orbitofrontal cortex	12.9 (9.72–32.4)	2.68 (2.11–3.28)
Left parahippocampal gyrus	24.5 (16.0–50.5)	5.14 (2.78–6.36)
Right parahippocampal gyrus	30.2 (21.0–77.9)	5.56 (2.25–10.1)
Left parietal lobe	9.27 (7.12–27.0)	1.26 (0.780–2.16)
Right parietal lobe	8.18 (5.90–21.4)	1.29 (0.822–2.19)
Left postcentral gyrus	9.52 (7.51–28.7)	1.40 (0.967–2.08)
Right postcentral gyrus	9.63 (5.31–18.2)	1.18 (0.844–2.24)
Left precentral gyrus	7.28 (5.98–21.1)	1.04 (0.913–1.50)
Right precentral gyrus	6.81 (4.97–16.8)	1.07 (0.707–1.73)
Left temporal lobe	16.9 (11.6–32.0)	2.89 (1.96–3.50)
Right temporal lobe	15.9 (11.7–34.1)	3.11 (2.24–3.74)
Left thalamus	4.30 (3.21–13.7)	0.996 (0.608–2.06)
Right thalamus	5.37 (3.59–11.3)	0.977 (0.734–1.98)
Left temporal pole*	15.0 (10.7–21.2)	2.67 (1.63–3.10)
Right temporal pole*	11.1 (8.42–26.9)	2.27 (1.53–3.65)
Brainstem	5.67 (4.01–10.3)	0.990 (0.654–1.52)

Note.—Data are median volume transfer constants (K^{trans}), with IQRs in parentheses.

* *Temporal pole* represents a region including the superior, middle, and inferior temporal gyrus and the temporal pole.

anti-NMDA receptor encephalitis (29 years [IQR, 26–36 years]) was younger than that of patients with anti-leucine-rich glioma-inactivated 1 encephalitis (63 years [IQR, 51–65 years]) ($P = .007$). Anti-leucine-rich glioma-inactivated 1 encephalitis had male predominance (male-to-female ratio, 5:2), while the anti-NMDA receptor subtype had female predominance (male-to-female ratio, 1:4).

Two patients with antibody-negative but probable autoimmune encephalitis without treatment and one patient with anti-NMDA receptor encephalitis without accessible electronic

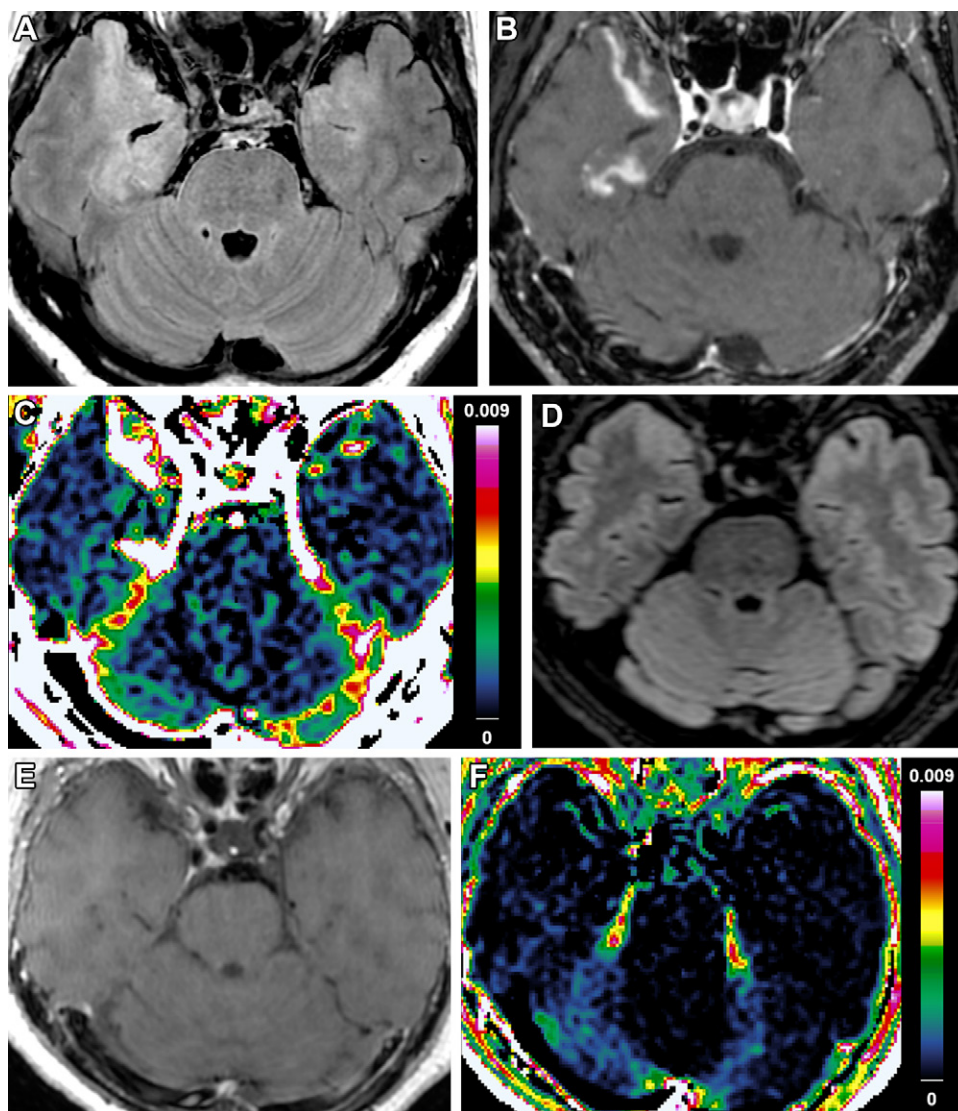


Figure 5: Representative (A) T2 fluid-attenuated inversion recovery image, (B) postcontrast T1-weighted image, and (C) volume transfer constant (K^{trans}) map in a patient with anti-leucine-rich glioma-inactivated 1 encephalitis (49-year-old man) with T2 hyperintensities in both temporal lobes, including the right parahippocampal gyrus, and (D–F) images acquired with the same protocols in a healthy control (70-year-old woman). The K^{trans} map in the patient (C) with focal lesions in both temporal lobes shows globally higher K^{trans} values as compared with the K^{trans} map in the healthy control (F) (pink: high K^{trans} ; blue: low K^{trans} [unit: min^{-1}]).

medical records were excluded from the treatment response analysis. Most patients in each subtype showed a good treatment response: 100% (seven of seven) with anti-leucine-rich glioma-inactivated 1 encephalitis, 78% (seven of nine) with anti-NMDA receptor encephalitis, and 79% (15 of 19) with antibody-negative but probable autoimmune encephalitis.

Comparison of Baseline K^{trans} Between Affected and Normal-appearing Regions at Structural MRI in Patients

Of the 38 patients, 12 had positive findings at structural MRI, with high signal intensity on T2 FLAIR images. The most frequently affected region was the left hippocampus and amygdala (Fig 3). Median values for patients with a focal lesion at the left hippocampus and amygdala and those without focal lesion were $7.39 \times 10^{-4} \text{ min}^{-1}$ (IQR, 5.11 – 10.7

$\times 10^{-4} \text{ min}^{-1}$) and $6.45 \times 10^{-4} \text{ min}^{-1}$ (IQR, 4.62 – $50.7 \times 10^{-4} \text{ min}^{-1}$), respectively ($P = .77$). T2 FLAIR hyperintense lesions with gyral or patchy contrast enhancement were found in eight patients, while T2 FLAIR hyperintense lesions without contrast enhancement were noted in four patients. There was no evidence of a difference between baseline K^{trans} value of T2 FLAIR hyperintense lesions with contrast enhancement (median, $21.7 \times 10^{-4} \text{ min}^{-1}$ [IQR, 4.31 – $60.8 \times 10^{-4} \text{ min}^{-1}$]) and those of T2 FLAIR hyperintense lesions without contrast enhancement (median, $9.84 \times 10^{-4} \text{ min}^{-1}$ [IQR, 6.99 – $17.2 \times 10^{-4} \text{ min}^{-1}$]) or normal-appearing regions (median, $7.40 \times 10^{-4} \text{ min}^{-1}$ [IQR, 5.73 – $12.0 \times 10^{-4} \text{ min}^{-1}$]) (adjusted $P > .99$ and $P = .60$ with the use of Bonferroni correction [$n = 3$]). There was no evidence of a difference between the K^{trans} value of MRI-detected abnormality, including both contrast-enhancing and nonenhancing portions of T2 FLAIR hyperintensity, and that of normal-appearing regions in the patients (median, $11.2 \times 10^{-4} \text{ min}^{-1}$ [IQR, 6.48 – $35.3 \times 10^{-4} \text{ min}^{-1}$] vs $7.40 \times 10^{-4} \text{ min}^{-1}$ [IQR, 5.73 – $12.0 \times 10^{-4} \text{ min}^{-1}$]; $P = .41$). The number of patients with positive findings in each subtype is presented in Figure S1. The number of patients with positive findings did not differ according to the subtypes (Table S3).

Comparison of Baseline K^{trans} Between Patients and Healthy Controls

All brain regions had higher baseline K^{trans} in patients as compared with healthy controls ($P < .001$ for all brain regions) (Tables 2, S4). The right parahippocampal gyrus had the largest median difference in K^{trans} as compared with the controls ($25.1 \times 10^{-4} \text{ min}^{-1}$ [95% CI: 17.6 , 43.4]) (Fig 4). Brain regions with the largest median difference of K^{trans} were the left parahippocampal gyrus ($25.9 \times 10^{-4} \text{ min}^{-1}$ [95% CI: 16.6 , 107]) in anti-NMDA receptor encephalitis, the right parahippocampal gyrus ($19.0 \times 10^{-4} \text{ min}^{-1}$ [95% CI: 10.4 , 27.4]) in anti-leucine-rich

glioma-inactivated 1 encephalitis, and the right parahippocampal gyrus ($30.1 \times 10^{-4} \text{ min}^{-1}$ [95% CI: 18.6, 70.4]) in antibody-negative but probable autoimmune encephalitis (Fig S2). Representative K^{trans} maps in a patient with autoimmune encephalitis and a healthy control are provided in Figure 5.

Fourteen of 38 patients underwent follow-up with DCE MRI within 2–6 months of their clinical course with treatment (steroid followed by intravenous immunoglobulin [$n = 7$] or steroid followed by intravenous immunoglobulin and immunosuppressant, including azathioprine, rituximab, and tocilizumab [$n = 7$]), and one patient underwent follow-up MRI without treatment. In paired comparison analysis, no evidence of changes in K^{trans} were found between baseline and follow-up in all brain regions ($P > .99$) (median, $39.4 \times 10^{-4} \text{ min}^{-1}$ [IQR, 26.6–91.1 $\times 10^{-4} \text{ min}^{-1}$] vs $28.5 \times 10^{-4} \text{ min}^{-1}$ [IQR, 21.3–108 $\times 10^{-4} \text{ min}^{-1}$] at the right parahippocampal gyrus) (Tables 3, S5).

Comparison of Baseline K^{trans} and Clinical Factors Between Good and Poor Treatment Response Groups

The treatment was individualized according to clinicians' decisions based on the patients' clinical disease manifestation, severity, comorbidity, and treatment response (Table S6). The poor treatment response group had higher baseline K^{trans} values in both cerebellar cortices ($P = .03$), the left cerebellar cortex ($P = .02$), right cerebellar cortex ($P = .045$), left cerebral cortex ($P = .045$), and left postcentral gyrus ($P = .03$) than the good treatment response group (Tables 4, S7; Fig 6). No evidence of differences between the good and poor treatment response groups was found with respect to the Anti-NMDA Receptor Encephalitis One-Year Functional Status score (median, 1 [IQR, 1–2] vs 3 [IQR, 1–3]; $P = .21$), age older than 60 years (24% [seven of 29 patients] vs 33% [two of six patients]; $P = .64$), infratentorial lesion at MRI (3% [one of 29] vs 0% [0

Table 3: Comparison of Baseline and Follow-up K^{trans} Values

Brain Region	Baseline ($\times 10^{-4} \text{ min}^{-1}$)	Follow-up ($\times 10^{-4} \text{ min}^{-1}$)
Left nucleus accumbens	8.40 (3.91–19.7)	6.45 (3.21–21.1)
Right nucleus accumbens	5.36 (4.31–26.5)	5.68 (4.64–41.2)
Left basal ganglia	4.21 (3.50–38.1)	5.27 (2.94–23.7)
Right basal ganglia	4.66 (3.97–41.8)	5.10 (3.09–21.4)
Left cerebellar cortex	11.7 (8.08–53.0)	8.51 (6.69–73.8)
Right cerebellar cortex	8.63 (6.80–55.4)	8.26 (5.34–77.7)
Left cerebellar white matter	4.12 (2.67–23.2)	3.64 (2.28–26.6)
Right cerebellar white matter	4.06 (3.07–29.8)	3.85 (2.21–21.4)
Left cerebral cortex	9.84 (8.37–61.9)	11.4 (8.87–57.5)
Right cerebral cortex	12.5 (8.75–54.7)	10.5 (8.60–69.0)
Left cerebral white matter	4.04 (2.93–19.2)	3.15 (2.16–21.6)
Right cerebral white matter	4.64 (2.78–20.6)	2.78 (2.18–21.6)
Left cingulate gyrus	11.1 (7.57–75.9)	7.99 (5.51–43.3)
Right cingulate gyrus	10.0 (9.12–92.5)	10.2 (7.50–70.3)
Left frontal lobe	8.29 (6.70–49.1)	7.84 (5.87–45.8)
Right frontal lobe	11.3 (6.98–51.7)	7.15 (5.31–53.8)
Left hippocampus and amygdala	6.95 (5.09–66.3)	6.40 (3.74–41.6)
Right hippocampus and amygdala	14.2 (4.84–68.6)	5.31 (4.19–43.4)
Left insula	8.37 (6.92–58.0)	9.65 (4.98–56.1)
Right insula	10.8 (5.71–79.5)	6.47 (4.61–51.7)
Left occipital lobe	25.7 (15.3–75.7)	17.3 (15.0–83.0)
Right occipital lobe	26.2 (18.0–90.9)	22.8 (14.2–104)
Left orbitofrontal cortex	17.8 (8.56–52.3)	13.3 (7.86–69.3)
Right orbitofrontal cortex	20.4 (10.9–57.1)	12.6 (8.27–77.8)
Left parahippocampal gyrus	30.3 (22.2–61.0)	24.9 (16.8–108)
Right parahippocampal gyrus	39.4 (26.6–91.1)	28.5 (21.3–108)
Left parietal lobe	9.22 (6.95–66.0)	9.25 (6.29–53.5)
Right parietal lobe	14.2 (6.16–60.2)	8.12 (6.45–54.7)
Left postcentral gyrus	9.68 (7.63–57.1)	9.15 (6.58–49.1)
Right postcentral gyrus	11.0 (5.73–57.2)	9.45 (6.42–47.3)
Left precentral gyrus	9.95 (6.29–48.4)	9.42 (7.03–42.3)
Right precentral gyrus	8.69 (5.55–50.2)	6.32 (5.16–49.3)
Left temporal lobe	17.5 (16.0–60.0)	15.8 (13.4–74.7)
Right temporal lobe	21.4 (13.2–80.2)	15.9 (12.0–103)
Left thalamus	4.22 (3.71–34.2)	4.42 (3.21–27.9)
Right thalamus	6.46 (4.28–42.7)	5.49 (3.62–26.8)
Left temporal pole*	17.3 (12.0–59.9)	14.8 (10.3–65.4)
Right temporal pole*	12.0 (8.99–73.5)	11.1 (8.0–89.1)
Brainstem	8.06 (4.40–35.0)	5.32 (3.48–40.9)

Note.—Data are median volume transfer constants (K^{trans}), with IQRs in parentheses.

* *Temporal pole* represents a region including the superior, middle, and inferior temporal gyrus and the temporal pole.

of six]; $P > .99$), and antibody subtype (cell-surface [anti-NMDA receptor and anti-leucine-rich glioma-inactivated 1 encephalitis]–to–antibody-negative but probable autoimmune encephalitis ratio, 14:15 vs 1:2; $P = .59$).

Correlation Between Baseline DCE MRI and Clinical Factors

At the right parahippocampal gyrus, no evidence of a significant correlation was found between the disease duration and baseline K^{trans} value ($\rho = 0.007$; $P = .97$). Baseline mRS scores showed no evidence of a significant correlation with K^{trans}

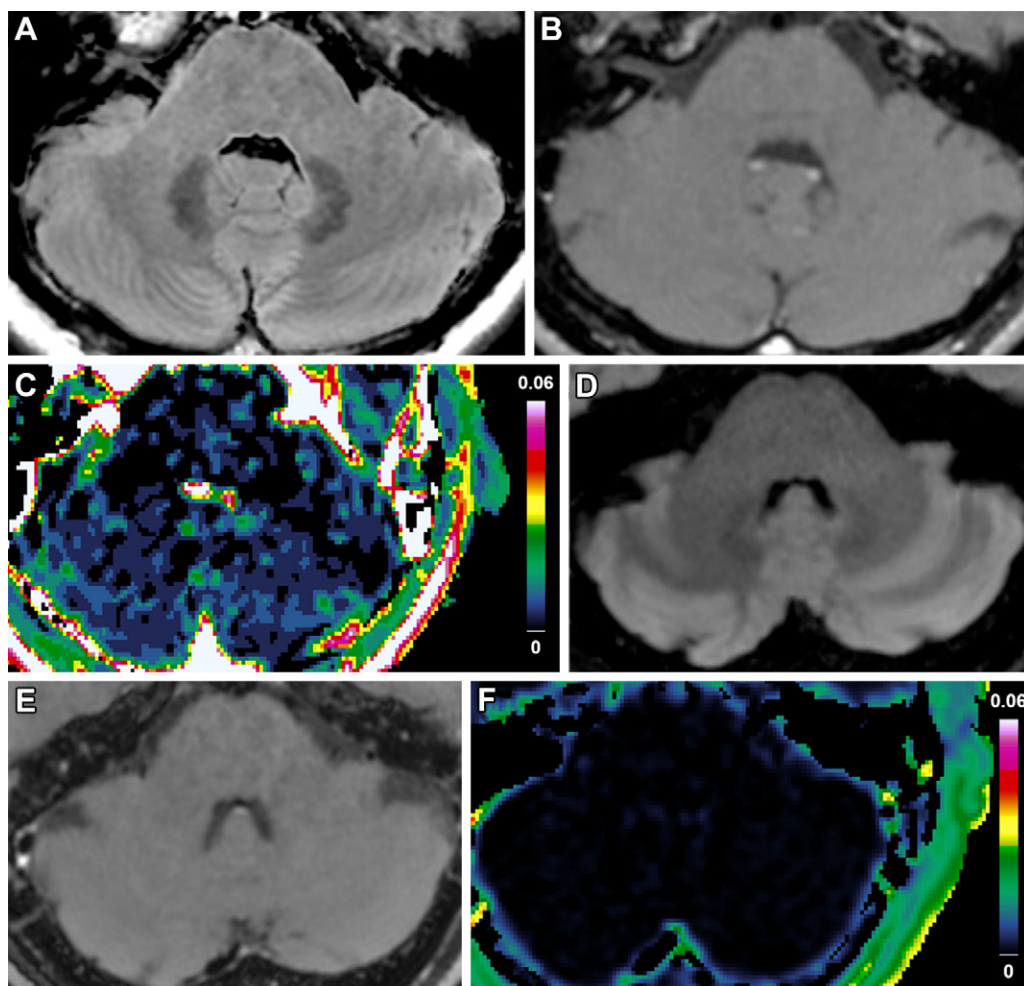


Figure 6: Representative (A) T2 fluid-attenuated inversion recovery image, (B) postcontrast T1-weighted image, and (C) volume transfer constant (K^{trans}) map in a 36-year-old female patient with anti-N-methyl-D-aspartate receptor encephalitis with poor treatment response and (D–F) images acquired with the same protocols in a 54-year-old female patient with antibody-negative but probable autoimmune encephalitis with good treatment response. The K^{trans} map in the patient with poor treatment response (C) shows higher K^{trans} values at both cerebellar cortices as compared with the K^{trans} map in the patient with good treatment response (F) (pink: high K^{trans} ; blue: low K^{trans} [unit: min^{-1}]).

values ($\rho = 0.115$; $P = .49$). Correlation results with other clinical factors are provided in Appendix S2.

Reproducibility of DCE MRI

Intraclass correlation coefficients of the whole-brain K^{trans} quantification were 0.53 (95% CI: 0.51, 0.55) for patients and 0.90 (95% CI: 0.89, 0.92) for controls.

Discussion

Previous studies suggest that blood-brain barrier (BBB) permeability change is a possible pathologic mechanism of autoimmune encephalitis (12–14,30,31). Our study provides additional evidence of globally increased BBB permeability in autoimmune encephalitis using dynamic contrast-enhanced MRI. In 38 patients with autoimmune encephalitis and 17 healthy controls, volume transfer constant (K^{trans}) values in all brain regions were higher in patients as compared with controls (largest median difference in the right parahippocampal gyrus [$25.1 \times 10^{-4} \text{ min}^{-1}$]). Among patients, poor

treatment responders had higher baseline K^{trans} values than good responders in both cerebellar cortices ($P = .03$), the left cerebellar cortex ($P = .02$), right cerebellar cortex ($P = .045$), left cerebral cortex ($P = .045$), and left post-central gyrus ($P = .03$).

Most previous studies on arterial spin labeling MRI findings of autoimmune encephalitis reported localized or diffuse hyperperfusion in affected or unaffected regions (32,33). A study investigating resting-state functional MRI and diffusion tensor imaging findings in anti-NMDA receptor encephalitis demonstrated reduced functional connectivity of both hippocampi with the anterior default mode network and extensive white matter changes, predominantly in the cingulum (34). As in previous studies (32–34), we also found extensively higher K^{trans} in all brain regions as compared with the controls,

including normal-appearing regions at structural MRI. This result highlights that autoimmune encephalitis, even with a negative structural MRI finding, can have increased permeability globally in the brain and that DCE MRI can be a helpful diagnostic tool in detecting early subtle changes in routine clinical practice. Of note, in our study, despite the term that suggests a pathologic abnormality limited to limbic brain, diffusely increased BBB permeability was commonly noted in the two subtypes of limbic encephalitis (anti-NMDA receptor and anti-leucine-rich glioma-inactivated 1 encephalitis). This result supports clinical and imaging findings indicating the involvement of a broad brain network in limbic encephalitis (35).

Liba et al (36) reported that T helper cell–related cytokines (interferon- γ , tumor necrosis factor- α , and interleukin-17A levels) and crucial cytokines for T-cell survival (interleukin-15) in cerebrospinal fluid were persistently increased during follow-up, despite the symptom improvement in most patients with anti-NMDA receptor encephalitis. These cytokines are

Table 4: Comparison of Regional K^{trans} Between Good and Poor Treatment Response Groups

Brain Region	Good Treatment Response ($\times 10^{-4} \text{ min}^{-1}$)	Poor Treatment Response ($\times 10^{-4} \text{ min}^{-1}$)	P Value
Left nucleus accumbens	5.14 (3.39–10.9)	20.1 (8.78–32.4)	>.99
Right nucleus accumbens	4.81 (3.83–8.39)	29.0 (10.6–49.8)	>.99
Left basal ganglia	3.70 (3.04–5.21)	30.7 (10.3–39.3)	.52
Right basal ganglia	4.08 (3.56–6.42)	42.6 (14.5–48.2)	.19
Left cerebellar cortex	8.86 (7.01–12.1)	61.4 (31.4–79.4)	.02
Right cerebellar cortex	7.23 (5.65–9.53)	59.3 (21.1–94.2)	.045
Left cerebellar white matter	3.16 (2.41–4.55)	22.1 (9.22–29.7)	.11
Right cerebellar white matter	3.32 (2.32–4.95)	22.7 (7.79–29.4)	.61
Left cerebral cortex	9.01 (8.09–14.8)	76.9 (32.5–86.6)	.045
Right cerebral cortex	9.14 (7.39–14.7)	79.4 (30.0–91.9)	.19
Left cerebral white matter	2.94 (2.41–4.04)	18.6 (7.59–21.8)	.27
Right cerebral white matter	2.98 (2.12–4.64)	20.0 (6.44–25.0)	>.99
Left cingulate gyrus	8.09 (5.52–14.5)	62.3 (21.6–79.5)	.94
Right cingulate gyrus	9.56 (7.48–14.3)	125 (34.8–162)	.19
Left frontal lobe	6.89 (5.83–11.4)	58.8 (23.9–66.8)	.09
Right frontal lobe	7.06 (5.19–10.8)	60.3 (20.9–71.1)	.27
Left hippocampus and amygdala	5.72 (4.62–7.96)	79.5 (19.9–107)	.38
Right hippocampus and amygdala	6.09 (4.32–12.6)	85.0 (25.4–103)	.32
Left insula	7.49 (5.39–8.72)	79.6 (24.8–119)	.82
Right insula	5.95 (4.18–11.2)	79.2 (26.4–97.0)	.32
Left occipital lobe	15.4 (14.4–24.1)	89.8 (36.0–122)	.27
Right occipital lobe	19.7 (16.2–26.3)	111 (46.0–146)	>.99
Left orbitofrontal cortex	10.6 (7.40–16.0)	73.7 (32.3–116)	.52
Right orbitofrontal cortex	11.5 (7.95–19.5)	77.5 (30.0–119)	.61
Left parahippocampal gyrus	23.4 (15.3–30.3)	108 (69.0–130)	.82
Right parahippocampal gyrus	27.7 (19.6–44.9)	117 (94.9–147)	.94
Left parietal lobe	7.90 (6.51–12.3)	78.6 (31.8–84.2)	.07
Right parietal lobe	7.10 (5.27–11.9)	73.1 (25.4–86.2)	.45
Left postcentral gyrus	8.39 (7.29–13.5)	79.4 (40.9–110)	.03
Right postcentral gyrus	7.50 (5.20–12.2)	65.5 (25.2–79.3)	>.99
Left precentral gyrus	6.80 (5.60–9.95)	57.5 (21.6–69.2)	.06
Right precentral gyrus	6.05 (3.85–8.69)	48.7 (18.3–66.7)	.19
Left temporal lobe	16.4 (11.2–19.4)	84.0 (41.3–104)	.23
Right temporal lobe	14.0 (11.1–21.4)	91.9 (42.7–109)	.71
Left thalamus	3.83 (2.89–5.40)	29.9 (12.1–35.8)	.27
Right thalamus	4.90 (3.36–6.46)	42.7 (14.0–58.5)	.27
Left temporal pole*	12.3 (9.75–16.0)	76.0 (28.5–98.7)	.61
Right temporal pole*	9.78 (7.97–12.0)	70.9 (35.9–97.3)	.45
Brainstem	4.66 (3.52–8.06)	28.5 (11.5–41.9)	.11

Note.—Unless otherwise specified, data are median volume transfer constants (K^{trans}), with IQRs in parentheses. *P* values were adjusted for multiple comparisons with the use of Bonferroni correction ($n = 58$).

* *Temporal pole* represents a region including the superior, middle, and inferior temporal gyrus and the temporal pole.

In terms of clinical outcome, higher baseline K^{trans} in the cerebellar cortex, left cerebral cortex, and left postcentral gyrus in the poor responders suggested that BBB was disrupted to a greater extent at baseline in the poor responders. Our finding is consistent with the previous finding that patients with damaged BBB, indicated by increased cerebrospinal fluid-to-serum quotient of albumin, had higher proportions of decreased consciousness and intensive care unit admission and ultimately higher mRS score at the 2-month follow-up examination (31).

Our study had several limitations. First, our patient sample size (especially those with poor treatment response and those with follow-up MRI) was small because not all patients with suspected autoimmune encephalitis underwent the dedicated MRI protocol, including DCE MRI. The lack of statistically significant associations between the K^{trans} value of the right parahippocampal gyrus and various clinical factors and the lack of statistically significant differences in clinical predictors of treatment response between good and poor responders may be partly attributable to the small sample size. Second, because of the retrospective nature of the study, the time interval between symptom onset and baseline imaging and the time interval between baseline and follow-up imaging varied among patients. Third, the healthy controls were not age- or sex-matched to the patients, and the healthy controls were

proinflammatory cytokines that play a role in BBB dysfunction by mediating reduction in tight junction expression or false tight junction allocation (37). Persistently elevated imaging, clinical, and pathologic markers reported in our study and previous studies suggest that autoimmune encephalitis may cause irreversible changes in BBB permeability in some patients.

considerably older than the patients. Fourth, as the slower leakage rate is one of the important factors in low-leakage (mild) diseases, the relatively short total sampling time (5 minutes 25 seconds for DCE MRI) may be suboptimal for accurate measurement of BBB permeability. Fifth, our study data were obtained on a single MRI scanner using a single software package.

A further multi-institutional study based on a larger number of patients and matched healthy controls is warranted to validate the generalizability of our findings. Sixth, K^{trans} values for both patients and controls were too small, and thus the possibility remains that changes observed could have been confounded by changes in signal-to-noise ratios.

In conclusion, dynamic contrast-enhanced (DCE) MRI demonstrated that blood-brain barrier permeability was increased in all brain regions in patients with autoimmune encephalitis, supporting the generalized nature of autoimmune encephalitis. Although it was difficult to provide a specific threshold to predict treatment response based on our limited data, higher baseline volume transfer constant values in the cerebellar cortex, left cerebral cortex, and left postcentral gyrus in poor treatment responders suggest that DCE MRI may serve as an objective basis for treatment response prediction in patients with autoimmune encephalitis and provide valuable information for counseling these patients about their prognosis.

Author contributions: Guarantors of integrity of entire study, S.H.J., R.E.Y., S.H.C.; study concepts/study design or data acquisition or data analysis/interpretation, all authors; manuscript drafting or manuscript revision for important intellectual content, all authors; approval of final version of submitted manuscript, all authors; agrees to ensure any questions related to the work are appropriately resolved, all authors; literature research, S.H.J., R.E.Y., S.H.C., W.J.L., S.T.L., I.H., T.J.Y.; clinical studies, S.H.J., R.E.Y., S.H.C., W.J.L., S.T.L., Y.H.J., J.Y.L., I.H., K.M.K., T.J.Y.; statistical analysis, S.H.J., R.E.Y., K.S.C., I.H.; and manuscript editing, S.H.J., R.E.Y., S.H.C., J.Y.L., T.J.Y.

Disclosures of conflicts of interest: S.H.J. No relevant relationships. R.E.Y. No relevant relationships. S.H.C. No relevant relationships. W.J.L. No relevant relationships. S.T.L. Grants to institution from Roche, GC Biopharma, and Celltrion; consulting fees from Roche. Y.H.J. No relevant relationships. K.S.C. No relevant relationships. J.Y.L. No relevant relationships. I.H. No relevant relationships. K.M.K. No relevant relationships. T.J.Y. No relevant relationships.

References

- Graus F, Titulaer MJ, Balu R, et al. A clinical approach to diagnosis of autoimmune encephalitis. *Lancet Neurol* 2016;15(4):391–404.
- Corsellis JA, Goldberg GJ, Norton AR. “Limbic encephalitis” and its association with carcinoma. *Brain* 1968;91(3):481–496.
- Dubey D, Pittock SJ, Kelly CR, et al. Autoimmune encephalitis epidemiology and a comparison to infectious encephalitis. *Ann Neurol* 2018;83(1):166–177.
- Zhang T, Duan Y, Ye J, et al. Brain MRI characteristics of patients with anti-N-methyl-D-aspartate receptor encephalitis and their associations with 2-year clinical outcome. *AJNR Am J Neuroradiol* 2018;39(5):824–829.
- Shan W, Yang H, Wang Q. Neuronal surface antibody-mediated autoimmune encephalitis (limbic encephalitis) in China: a multiple-center, retrospective study. *Front Immunol* 2021;12:621599.
- Qiao S, Wu HK, Liu LL, et al. Characteristics and prognosis of autoimmune encephalitis in the east of China: a multi-center study. *Front Neurol* 2021;12:642078.
- Gable MS, Sheriff H, Dalmau J, Tilley DH, Glaser CA. The frequency of autoimmune N-methyl-D-aspartate receptor encephalitis surpasses that of individual viral etiologies in young individuals enrolled in the California Encephalitis Project. *Clin Infect Dis* 2012;54(7):899–904.
- Bien CG, Vincent A, Barnett MH, et al. Immunopathology of autoantibody-associated encephalitis: clues for pathogenesis. *Brain* 2012;135(Pt 5):1622–1638.
- Dalmau J, Armangué T, Planagumà J, et al. An update on anti-NMDA receptor encephalitis for neurologists and psychiatrists: mechanisms and models. *Lancet Neurol* 2019;18(11):1045–1057.
- Moscatto EH, Peng X, Jain A, Parsons TD, Dalmau J, Balice-Gordon RJ. Acute mechanisms underlying antibody effects in anti-N-methyl-D-aspartate receptor encephalitis. *Ann Neurol* 2014;76(1):108–119.
- Da Mesquita S, Fu Z, Kipnis J. The meningeal lymphatic system: a new player in neurophysiology. *Neuron* 2018;100(2):375–388.
- Hammer C, Stepniak B, Schneider A, et al. Neuropsychiatric disease relevance of circulating anti-NMDA receptor autoantibodies depends on blood-brain barrier integrity. *Mol Psychiatry* 2014;19(10):1143–1149.
- Martinez-Hernandez E, Horvath J, Shiloh-Malawsky Y, Sangha N, Martinez-Lage M, Dalmau J. Analysis of complement and plasma cells in the brain of patients with anti-NMDAR encephalitis. *Neurology* 2011;77(6):589–593.
- Platt MP, Bolding KA, Wayne CR, et al. Th17 lymphocytes drive vascular and neuronal deficits in a mouse model of postinfectious autoimmune encephalitis. *Proc Natl Acad Sci U S A* 2020;117(12):6708–6716.
- Schläger C, Körner H, Krueger M, et al. Effector T-cell trafficking between the leptomeninges and the cerebrospinal fluid. *Nature* 2016;530(7590):349–353.
- Tavares GA, Louveau A. Meningeal lymphatics: an immune gateway for the central nervous system. *Cells* 2021;10(12):3385.
- Sourbron S, Ingrisch M, Siefert A, Reiser M, Herrmann K. Quantification of cerebral blood flow, cerebral blood volume, and blood-brain-barrier leakage with DCE-MRI. *Magn Reson Med* 2009;62(1):205–217.
- Sourbron SP, Buckley DL. Classic models for dynamic contrast-enhanced MRI. *NMR Biomed* 2013;26(8):1004–1027.
- Chagnot A, Barnes SR, Montagne A. Magnetic resonance imaging of blood-brain barrier permeability in dementia. *Neuroscience* 2021;474:14–29.
- Cramer SP, Larsson HB. Accurate determination of blood-brain barrier permeability using dynamic contrast-enhanced T1-weighted MRI: a simulation and in vivo study on healthy subjects and multiple sclerosis patients. *J Cereb Blood Flow Metab* 2014;34(10):1655–1665.
- Jung SC, Yeom JA, Kim JH, et al. Glioma: application of histogram analysis of pharmacokinetic parameters from T1-weighted dynamic contrast-enhanced MR imaging to tumor grading. *AJNR Am J Neuroradiol* 2014;35(6):1103–1110.
- Kim YS, Kim M, Choi SH, et al. Altered vascular permeability in migraine-associated brain regions: evaluation with dynamic contrast-enhanced MRI. *Radiology* 2019;292(3):713–720.
- Yoen H, Yoo RE, Choi SH, et al. Blood-brain barrier disruption in mild traumatic brain injury patients with post-concussion syndrome: evaluation with region-based quantification of dynamic contrast-enhanced MR imaging parameters using automatic whole-brain segmentation. *Korean J Radiol* 2021;22(1):118–130.
- Lee WJ, Lee ST, Moon J, et al. Tocilizumab in autoimmune encephalitis refractory to rituximab: an institutional cohort study. *Neurotherapeutics* 2016;13(4):824–832.
- Li H, Liu X, Wang R, et al. Blood-brain barrier damage and new onset refractory status epilepticus: an exploratory study using dynamic contrast-enhanced magnetic resonance imaging. *Epilepsia* 2023;64(6):1594–1604.
- Wan X, Wang W, Liu J, Tong T. Estimating the sample mean and standard deviation from the sample size, median, range and/or interquartile range. *BMC Med Res Methodol* 2014;14(1):135.
- Schacht A, Bogaerts K, Bluhmki E, Lesaffre E. A new nonparametric approach for baseline covariate adjustment for two-group comparative studies. *Biometrics* 2008;64(4):1110–1116.
- Balu R, McCracken L, Lancaster E, Graus F, Dalmau J, Titulaer MJ. A score that predicts 1-year functional status in patients with anti-NMDA receptor encephalitis. *Neurology* 2019;92(3):e244–e252.
- Lee WJ, Lee HS, Kim DY, et al. Seronegative autoimmune encephalitis: clinical characteristics and factors associated with outcomes. *Brain* 2022;145(10):3509–3521.
- Platt MP, Agalliu D, Cutforth T. Hello from the other side: how autoantibodies circumvent the blood-brain barrier in autoimmune encephalitis. *Front Immunol* 2017;8:442.
- Yu Y, Wu Y, Cao X, et al. The clinical features and prognosis of anti-NMDAR encephalitis depends on blood brain barrier integrity. *Mult Scler Relat Disord* 2021;47:102604.
- Li R, Jin S, Wang Y, et al. Brain perfusion alterations on 3D pseudocontinuous arterial spin-labeling MR imaging in patients with autoimmune encephalitis: a case series and literature review. *AJNR Am J Neuroradiol* 2022;43(5):701–706.
- Sachs JR, Zapadka ME, Popli GS, Burdette JH. Arterial spin labeling perfusion imaging demonstrates cerebral hyperperfusion in anti-NMDAR encephalitis. *Radiol Case Rep* 2017;12(4):833–837.
- Finke C, Kopp UA, Scheel M, et al. Functional and structural brain changes in anti-N-methyl-D-aspartate receptor encephalitis. *Ann Neurol* 2013;74(2):284–296.
- Navarro V, Kas A, Apartis E, et al. Motor cortex and hippocampus are the two main cortical targets in LGI1-antibody encephalitis. *Brain* 2016;139(Pt 4):1079–1093.
- Liba Z, Kayserova J, Elisak M, et al. Anti-N-methyl-D-aspartate receptor encephalitis: the clinical course in light of the chemokine and cytokine levels in cerebrospinal fluid. *J Neuroinflammation* 2016;13(1):55.
- Huang X, Hussain B, Chang J. Peripheral inflammation and blood-brain barrier disruption: effects and mechanisms. *CNS Neurosci Ther* 2021;27(1):36–47.